



# The Electrochemical Corrosion Behavior of Plasma Electrolytic Oxidation Coatings Fabricated on Aluminum in Silicate Electrolyte

Zhong Yang, Rui-qiang Wang, Chen Liu, Ye-kang Wu, Dong-dong Wang, Xin-tong Liu, Xu-zhen Zhang, Guo-rui Wu, and De-jiu Shen

(Submitted May 23, 2018; in revised form March 19, 2019; published online May 15, 2019)

Plasma electrolytic oxidation (PEO) coatings were fabricated on the aluminum in silicate electrolyte. Microstructures and elemental compositions of these PEO coatings were examined by scanning electron microscopy (SEM) equipped with an energy-dispersive x-ray spectroscopy (EDS). Corrosion resistances of the coated samples were evaluated using the measurements of open-circuit potential (OCP), repetitive polarization and electrochemical impedance spectroscopy (EIS) in 3.5 wt.% NaCl solution. The results indicated that the PEO coatings not only act as a physical shield limiting the penetration of corrosive solution, but also establish an anodic location with high concentration of  $H^+$  ions and other product ions as pitting corrosion begins. With the development of pitting corrosion, the accumulation of corrosion products inside the pits and pores of the coatings decreases the corrosion process effectively.

**Keywords** aluminum, coatings, EIS, inorganic, interface, pitting corrosion, plasma electrolytic oxidation

## 1. Introduction

A various coating technologies have been developed to improve the corrosion and wear resistance of pure aluminum and its alloys. Among them, plasma electrolytic oxidation (PEO) has recently attracted enormous attention as a relatively new surface modification technique, in which a thick ceramic-like oxide coating could be developed in situ on valve metals (magnesium, aluminum, titanium, etc.). And as a conversion coating involving a mass of electrolyte elements, the PEO coating provides a considerable corrosion resistance (Ref 1-4). On the other hand, the thickness and the hardness of PEO coatings are much greater than those of conventional anodic films, and the PEO coatings also show a good adhesion to the substrates due to the complex hybrid reactions, involving an intricate combination of electrochemical, thermochemical, plasma-chemical and metallurgical reactions, and these interactions mainly occur on the interfaces, resulting in the PEO coatings on the metal surface composed of both the elements from the electrolyte and the substrate material (Ref 5-8). However, due to the existence of plasma discharge, gas liberation and energy generation, there are usually numerous

defects in the coatings, for instance, pores and cracks (Ref 7), which are detrimental to the anti-corrosion performance.

It is evident that the corrosion resistance of PEO-coated metals will experience a degradation process during long-term immersion test in chloride solution due to the penetration of corrosive solution through the porous microstructures in the coatings (Ref 9, 10). Based on the understanding of corrosion mechanisms of PEO-coated metals, extensive researches have been carried out to investigate the factors that affect the corrosion resistance performance of the PEO coatings, e.g., coating compositions, microstructures (Ref 11, 12), barrier layer properties (Ref 13), chloride ion concentration (Ref 5) and pH values of the corrosive solution (Ref 14). In addition, new electrical parameters (Ref 15), electrolyte compositions (Ref 16-18) and pre-treatments (Ref 19) have also been developed to enhance the corrosion resistance of the PEO coatings. Another important method to improve the corrosion resistance of PEO coatings is sealing post-treatment resulting from the porous microstructure of these coatings (Ref 20, 21).

To better understand the corrosion characteristics of the PEO-coated metals, various electrochemical tests have been employed in recent works (Ref 22, 23). Among them, electrochemical impedance spectroscopy (EIS) is the most frequently used method by which more dynamic information and interface structural information could be obtained (Ref 24). Although the resultant EIS plots are varied due to the complex geometries of the samples, electrochemical reactions and corrosion evolution in the PEO coatings, a typical two-layer structure has been used to describe the corrosion characteristics of the PEO-coated metals, i.e., the porous outer layer and the compact inner layer (Ref 5, 10). Furthermore, other electrochemical tests have been performed; for example, H. Duan used the value of capacitance of PEO specimens to investigate their semiconducting property associated with corrosion resistance (Ref 11).

The effect of PEO coatings is normally regarded as a physical shield which plays a role of limiting the penetration process of corrosive medium and restraining the anodic partial

Zhong Yang, Rui-qiang Wang, Chen Liu, Ye-kang Wu, Dong-dong Wang, Xin-tong Liu, Xu-zhen Zhang, and De-jiu Shen, State Key Laboratory of Metastable Materials Science and Technology, College of Materials Science and Engineering, Yanshan University, Qinhuangdao 066004, P. R. China; Guo-rui Wu, State Key Laboratory of Metastable Materials Science and Technology, College of Materials Science and Engineering, Yanshan University, Qinhuangdao 066004, P. R. China; and CITIC Dicastal Limited by Share Ltd, Qinhuangdao 066000, P. R. China. Contact e-mail: DejiuShen@163.com.

reactions in electrochemical corrosion process (Ref 25). However, the effects of the coating on the pitting corrosion, especially on the internal environment of pits, are seldom discussed. In the current work, besides the traditional OCP and EIS measurements, repetitive polarization method is employed to make a kind of “artificial pit” to investigate the transfer process of ions in the pits. On the basis of stage features of the corrosion process of the PEO-coated aluminum during a long-term immersion test in 3.5 wt.% NaCl solution, the various effects of pores on the corrosion process of the PEO coatings are discussed.

## 2. Experimental

### 2.1 Preparation of PEO Coatings

A sheet of AA1060 pure aluminum (0.05% Cu, 0.03% Mn, 0.03% Mg, 0.05% Zn, 0.03% Ti, 0.25% Si, 0.35% Fe, 0.05% V and Al balance) was cut into specimens with the dimensions of 15 mm × 15 mm × 1.5 mm as the substrate for the PEO treatment. Before the PEO treatment, all the specimens were ground successively with 500, 800 and 1200 grit emery sheets and degreased ultrasonically in acetone, cleaned in distilled water and then dried in a warm air system. PEO treatment was performed by a homemade experimental setup with an asymmetric AC power supply of 20 kW. The electrolyte for PEO process consists of 0.03 mol/L sodium silicate and 0.05 mol/L sodium hydroxide. PEO specimens were treated in a constant current density of 44 mA/cm<sup>2</sup> for 15 min, and the temperature of the electrolyte was kept at 298 ± 2 K by a water cooling system.

### 2.2 Electrochemical Tests and Analysis

Long-term immersion tests of the specimens were carried out in 3.5 wt.% NaCl solution (pH 7.0) at room temperature. The specimens were immersed for different durations, viz. 1, 5, 10, 15, 20, 40, 150 and 720 h, to understand the degradation process of the PEO specimens. Electrochemical tests were performed using a RST5000 electrochemical workstation with a typical three-electrode cell setup, saturated calomel reference electrode, platinum plate counter electrode and PEO-coated specimen as the working electrode with an exposed area of 0.5 cm<sup>2</sup>. Three different electrochemical tests were performed in the NaCl solution, i.e., open-circuit potential (OCP), repetitive polarization and electrochemical impedance spectroscopy (EIS). The OCP of the specimen was measured to characterize the initial electrochemical state evolution of the specimen. The repetitive polarization test of twelve cycles with potential ranging from −1.6 to 0.2 V at a sweep rate of 1 mV/s was carried out to investigate the transfer state of ions in the pits during electrochemical corrosion by means of fabricating a kind of artificial pits. The EIS measurements were carried out from a start frequency of 10<sup>5</sup> Hz to an end frequency of 10<sup>−2</sup> Hz with a disturbing potential of 5 mV. ZSimpWin software was used for the data fitting of impedance spectroscopy (Version 3.0, USA). The Chi-squared ( $\chi^2$ ) values of the fitting results, less than 5 × 10<sup>−3</sup>, were employed to evaluate the fitting quality, which indicate that the obtained data were consistent with the proposed equivalent circuit. Surface, cross-sectional morphologies, and chemical compositions of PEO specimens before and after immersion for different

durations were examined by a scanning electron microscopy (SEM, Hitachi S-4800) equipped with an energy-dispersive x-ray spectrometer (EDS). For the purpose of investigating the coating/substrate(C/S) interface, a series of coatings were detached from the substrates by using an electrochemical technique (Ref 26, 27). After detachment, the coatings were soaked in deionized water to remove the residual particles adhering to the coatings, and then dried in the drying vessel.

## 3. Results and Discussion

### 3.1 Long-Term Immersion Test

Specimens are immersed in 3.5 wt.% NaCl solution for different time durations to study the degradation process of the PEO coatings. Electrolyte/coating (E/C) interface and cross-sectional morphologies of the PEO specimens before and after 40- and 720-h immersion are both shown in Fig. 1. From Fig. 1(a), it can be seen that there are two sorts of distinct regions on the E/C interface of the un-immersed PEO samples, flat pancake regions (region “A”) with a central pore and some cracks, and the nodular regions (region “B”) around the pancakes, which are typical features for the PEO coatings formed on aluminum and its alloys in diluted silicate electrolytes (Ref 28). The pores and cracks are inevitable on the coating surface due to the existence of plasma discharges, gas liberations and thermal processes. These pores and cracks normally do not directly connect with the metal surface because there is a continuous and compact amorphous alumina layer region covering the metal surface. The EDS results shown in Table 1 illustrate that the flat pancake regions are rich in aluminum while the nodular regions are rich in silicon. The differences in morphology and chemical compositions between the two regions may be due to the different discharge types during the PEO process (Ref 29). After 40-h immersion, the E/C interface morphology of the specimen, as shown in Fig. 1(b), experienced little change in comparison with the original morphology. Although the two typical regions of the coating are still retained, it can be observed from Fig. 1(c) that the pancake regions become uneven after 720-h immersion treatment. In addition, some original flat regions around the central pores have turned into low-lying areas after the immersion treatment, but no peeling off or corroded cavity could be observed on the E/C interface. Furthermore, it should be noted that some pores in the immersed coating are filled with some corrosion products, e.g., region “C,” as shown in Fig. 1(c). The EDS results of region “C,” shown in Table 1, illustrate that the Al/O atomic ratio of the corrosion products is 0.36, which is close to that of Al(OH)<sub>3</sub>, and is different from those regions of “A” and “B” on the E/C interface of the un-immersed samples. The Cl and Na elements in the corrosion products of region “C” come from the corrosive solution. Figure 1(d), (e), and (f) is the cross-sectional images of the PEO specimens before immersion treatment, and after 40- and 720-h immersion treatment, respectively. Pores, near the inner section of the coating, can be observed in the un-immersed specimen (Fig. 1d), which reveals the porosity of the PEO coatings. After 40-h immersion, as shown in Fig. 1(e), some corrosion pits can be observed underneath the coating surface although the morphology of the coating surface changed little. The EDS results of region “D” show some Cl and Na elements and a

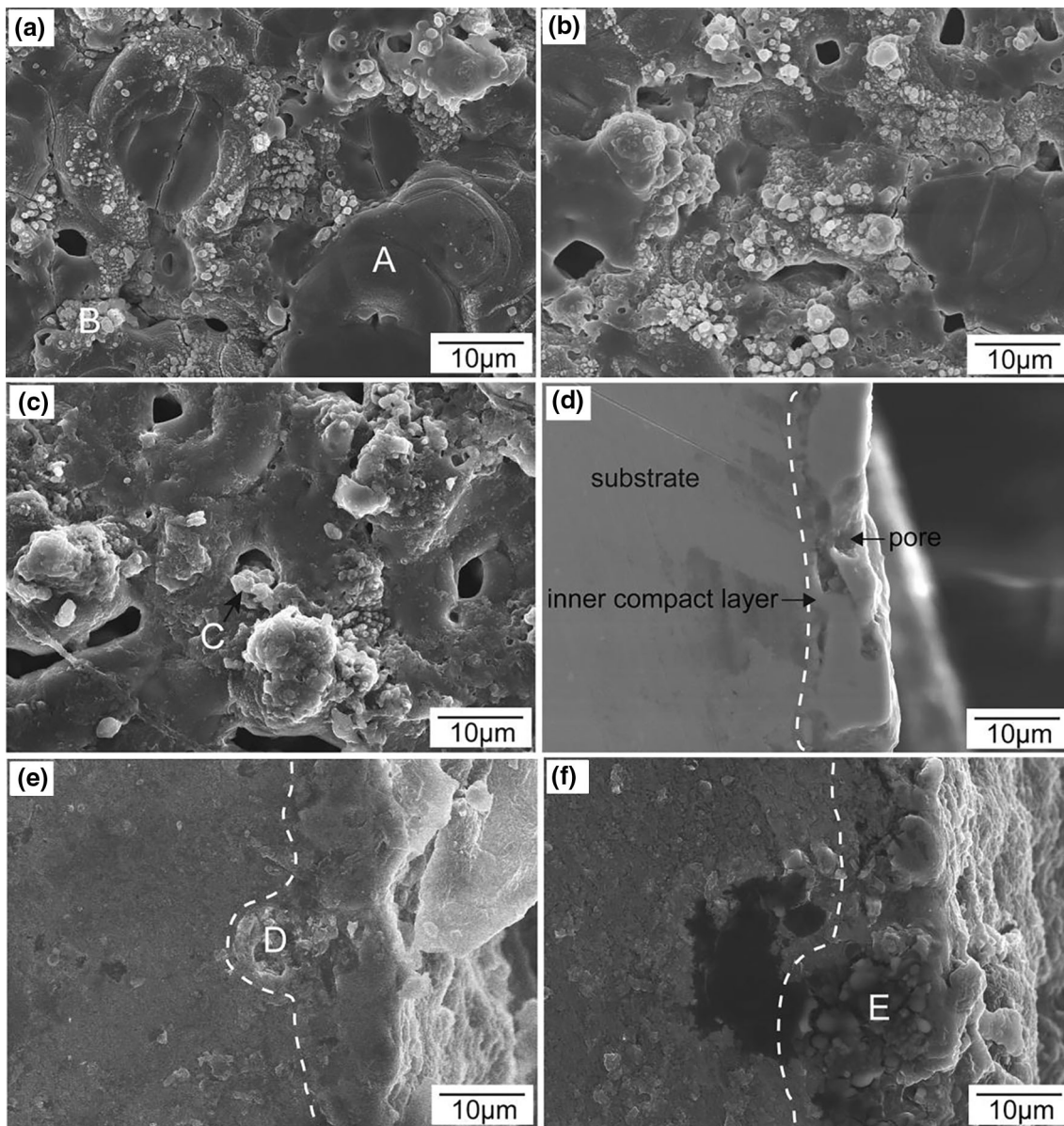


**Fig. 1** Electrolyte/coating (E/C) interface and cross-sectional morphologies of PEO coatings before and after immersion in 3.5 wt.% NaCl solution. (a) E/C interface before immersion; (b) E/C interface after 40-h immersion; (c) E/C interface after 720-h immersion; (d) cross section before immersion; (e) cross section after 40-h immersion; (f) cross section after 720-h immersion

**Table 1** EDS results of the regions in Fig. 1

Region	O, at.%	Al, at.%	Si, at.%	Cl, at.%	Na, at.%
A	58.16	40.14	1.7	...	...
B	70.52	4.74	24.74	...	...
C	54.53	19.80	3.00	9.49	13.18
D	46.59	49.35	...	2.02	2.04
E	73.14	25.49	0.61	0.76	...

high O content (46.59%) compared to the substrate, indicating this region has been corroded. The Al/O atomic ratio of region “D” is higher than that of region “C”, which may be due to the fact that the corrosion products layer is thin on the cross section of the pits; hence, the Al substrate under the corrosion products can be detected. In the cross-sectional image of the specimen

immersed for 720 h, deeper pits are found beneath the coating, as depicted in Fig. 1(f). Some pustule-like corrosion products are deposited in some pits, as region “E,” and the EDS results reveal that the Al/O atomic ratio of the corrosion products in these areas is 0.35, similar to that of region “C.”

The morphologies of coating/substrate (C/S) interface before and after different durations of immersion treatment are displayed in Fig. 2. The large protuberance structures indicate that intense reactions have occurred and gone deeper into the substrate during the PEO process. The transmission electron microscopy (TEM) results disclose that there is always a thin ( $< 1 \mu\text{m}$ ) amorphous alumina layer covering the metal substrate (Ref 30, 31), suggesting that the C/S interface with hemispherical oxides is composed of the direct PEO products resulting from plasma discharges occurring at the substrate surface and the size of hemispherical oxides represents the size of the plasma discharge areas here (Ref 26, 32). It

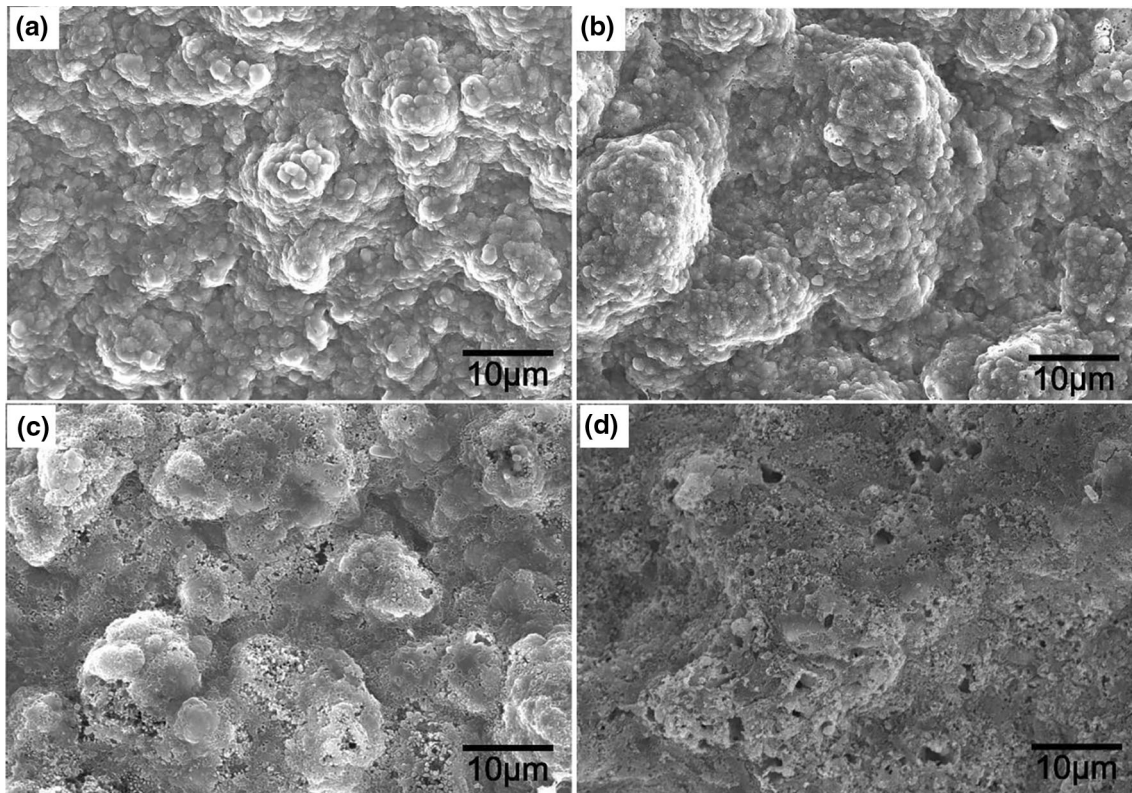


**Fig. 2** Coating/substrate (C/S) interface morphologies of PEO coatings before and after immersion in 3.5 wt.% NaCl solution: (a) C/S interface before immersion; (b) C/S interface after 10-h immersion; (c) C/S interface after 40-h immersion; (d) C/S interface after 720-h immersion

can be seen that the PEO coating has no distinct corrosion damage after 10-h immersion treatment in the NaCl solution, suggesting that the corrosive solution has not penetrated the C/S interface. Marked difference occurs after the 40-h immersion treatment, and the hemispherical oxides have been damaged. It is obvious that the corrosive medium has already infiltrated into the C/S interface. The typical morphologies of hemispherical oxides virtually disappear after 720-h corrosion treatment, indicating that the corrosive solution has completely penetrated the PEO coating and arrived at the substrate surface after 720-h corrosion experiment.

### 3.2 Electrochemical Tests

**3.2.1 Open-Circuit Potential Measurement.** Open-circuit potential (OCP) measurement is generally carried out to investigate the chemical stability and corrosion thermodynamics of the surface layer of the PEO-coated metals (Ref 2). The OCP of the PEO specimen in 3.5 wt.% NaCl solution as a function of immersion time is shown in Fig. 3. Once the PEO specimen is immersed into the NaCl solution, the solution begins to penetrate into the coatings through the channels of the pores and cracks in the coatings as shown in Fig. 1(a) and (d). From the curve, it can be seen that this process lasts up to 20-h immersion, and the main effect of the PEO coating in this stage is a physical shield that restricts the penetration evolution of the corrosive solution. Things begin to change from about 20 to 33 h, the OCP relatively stabilizes at a certain level of about  $-800$  mV, suggesting that the concentration gradient of the corrosive solution in the coatings vanishes after sufficient immersion time. In fact, the OCP curve fluctuates within

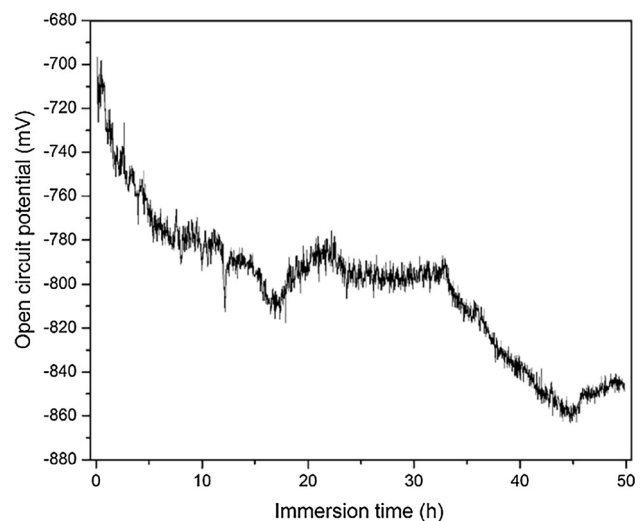


**Fig. 3** Open-circuit potential of PEO specimen in 3.5 wt.% NaCl solution

considerable amplitude instead of maintaining at a relatively stable value, indicating that it is difficult for the polarization processes on the surface of the PEO specimen to be an equilibrium state. Then, the OCP experiences another stage, decreasing from  $-800$  to  $-860$  mV for about 12 h. This decrease may be induced by pitting corrosion because some pits are found on the cross section of the specimen immersed for 40 h (Fig. 1e), and the inner surface of the sample immersed for 40 h in aggressive solution has begun to be damaged

(Fig. 2c). It should be noted that the OCP of the PEO specimen is relatively noisy throughout the whole measurement. The factors for this phenomenon are various, e.g., chemical dissolution, solution penetration, electrochemical corrosion, temperature fluctuation and pH change induced by the corrosion, etc., and these all are able to result in the state change in the sample surface.

**3.2.2 Electrochemical Impedance Spectroscopy.** Electrochemical impedance spectroscopy (EIS) is conducted to study the degradation process of the barrier properties of the PEO coatings during the immersion experiment. Figure 4 shows the Nyquist and Bode plots of the coated specimen immersed in 3.5 wt.% NaCl solution for different time durations. It has been known that the impedance data in high-frequency region reveal the corrosion characteristics of the outer layer of the coating while the data in low-frequency region show the barrier layer ones (Ref 33). The Nyquist plots shown in Fig. 4(a), (d), and (g) show two capacitive loops except the specimen immersed for 720 h, and the diameter of capacitive loop corresponding to low frequency is much larger

than that of high frequency. As shown in the Bode plots in Fig. 4(b), (c), (e), and (f), it is noticed that the impedance ( $|Z|$  value) in low-frequency region is evidently higher than that in high-frequency region.

Taking into account the microstructure characteristics of the coating, the electrical schematic representations of the coatings and the corresponding equivalent circuits (EC) are proposed in Fig. 5, which have also been proposed by the other researches (Ref 5). In these circuits,  $R_s$ ,  $R_1$ ,  $R_2$  and  $R_L$  are the resistance of the solution, the resistance of the defects (pores and cracks) in the coatings, the charge-transfer resistance on the surface of aluminum and the inductive resistance of adsorption of species in corrosion pits, respectively. Because of the non-ideal dielectric properties of the coatings, constant phase element (CPE) is employed instead of capacitive element (C) to reflect the inhomogeneity, roughness and porosity of the coatings. In the circuits,  $CPE_1$  presents the capacitance of the passive film and  $CPE_2$  presents the double-layer capacitance of the substrate surface.  $Z_W$  is the Warburg component which is associated with the diffusion processes of ions in the porous coatings. The

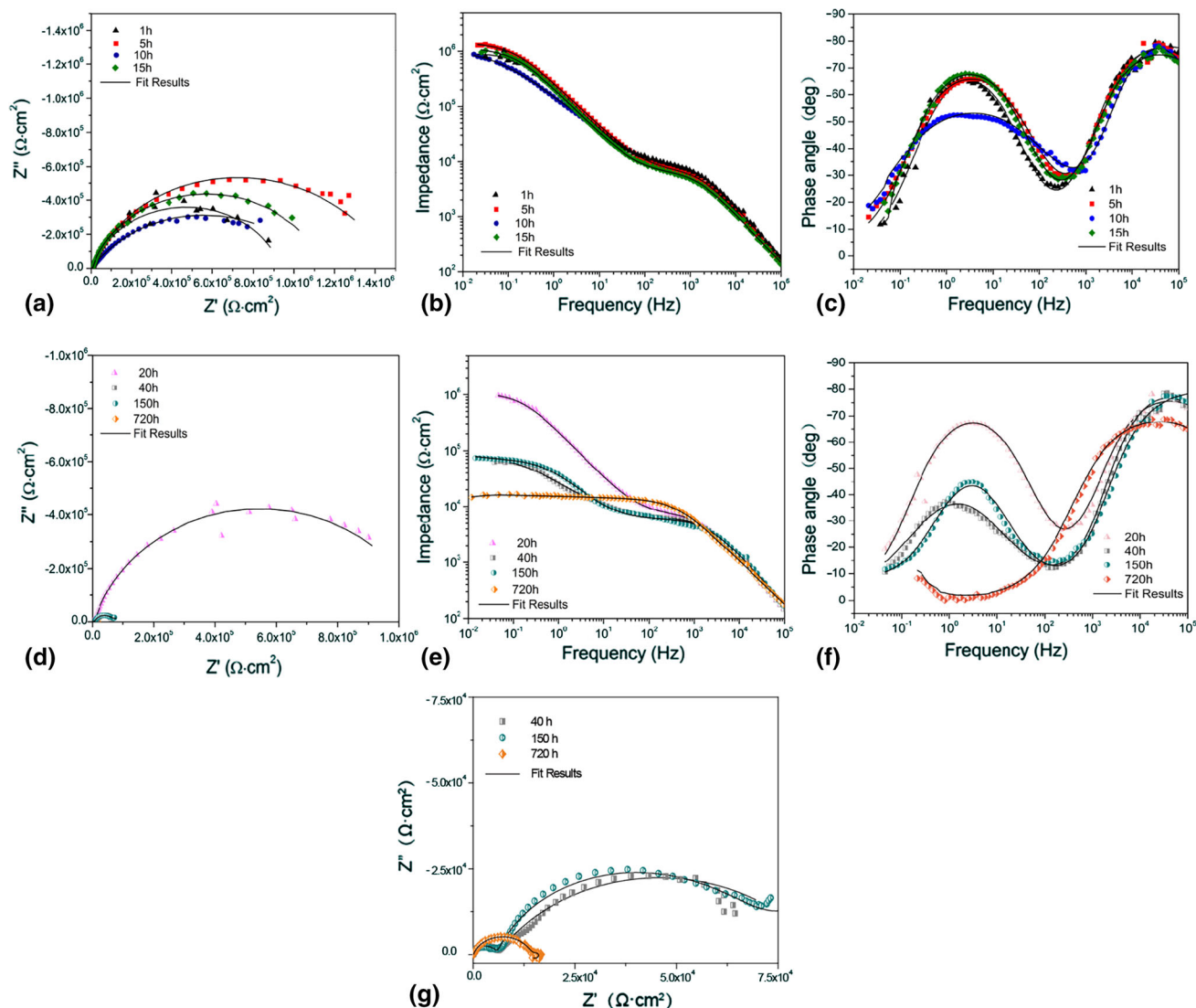


**Fig. 4** Electrochemical impedance behavior of PEO-coated aluminum specimens in 3.5 wt.% NaCl solution (after different durations of immersion). (a, d) Nyquist plots; (b, c, e, f) Bode plots; (g) a magnified image of Nyquist plots after 40-, 150- and 720-h immersion

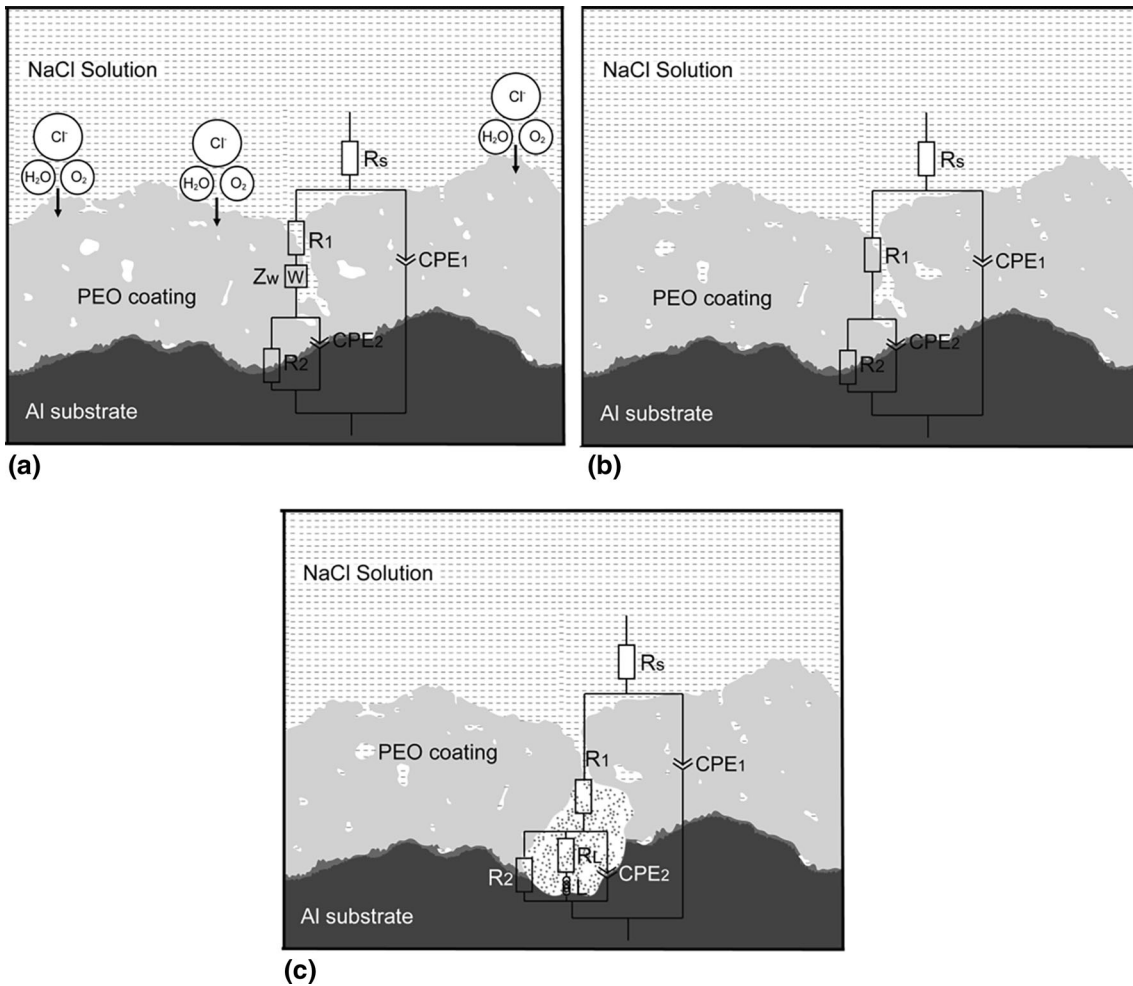


**Fig. 5** Schematic representation of the corrosion process of PEO-coated aluminum with equivalent circuits during long-term immersion in 3.5 wt.% NaCl solution: (a) solution penetration stage; (b) pitting corrosion stage; (c) corrosion products accumulation stage

inductive element  $L$  is associated with the relaxation processes involving the dissolution of the metal and the pitting corrosion of Al substrate.

Keqin Du et al. (Ref 10) investigated the water transport process through PEO coatings on aluminum substrate during the initial stage of immersion by EIS technique and concluded that the transport of corrosive solution through the PEO coating was like a diffusion process, especially for the inner layer. In the present work, the EIS plots of 1, 5, 10, 15 and 20 h, which is corresponding to the EC in Fig. 5(a), illustrate the diffusion process in the coating during the first 20-h immersion. As the pores and cracks in the coatings are infiltrated by the solution, the value of  $R_1$  decreases rapidly in the first 20-h immersion treatment as shown in Fig. 6, which also proves the penetration process of the corrosive solution. During this period, the contact of the corrosive solution and the substrate is inadequate because the transfer of the corrosive solution is limited by the coatings, especially the compact inner barrier layer.

After sufficient immersion time, the PEO coatings are saturated with the corrosive solution and some regions of the substrate under the defects of the coating contact with the corrosive solution sufficiently, and these regions become vulnerable regions and begin to be corroded. The EC corresponding to plots of 40 and 150 h changes into Fig. 5(b). An

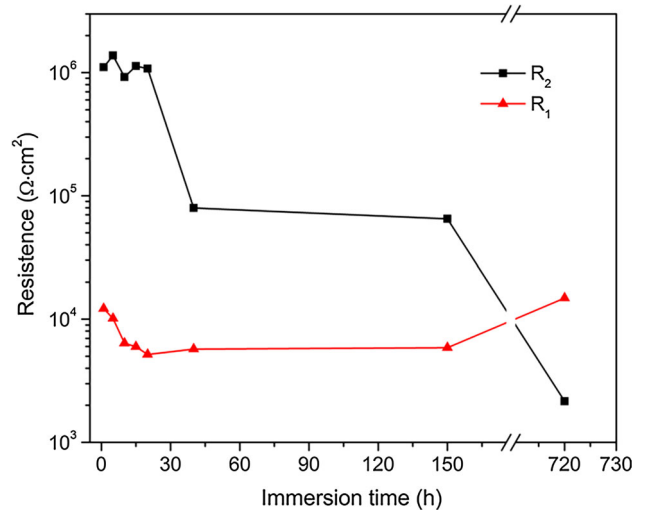
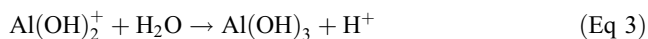
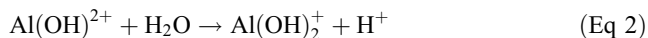


**Fig. 6** Values of fitted parameters  $R_1$  and  $R_2$  of the equivalent circuits

evident decline of the impedance value in low frequency occurs between 20 and 40 h, revealing the beginning of the damage of C/S interface, as shown in Fig. 4(d), (e) and 6.

The anodic dissolution of the Al substrate in some vulnerable regions is established:  $\text{Al} \rightarrow \text{Al}^{3+} + 3\text{e}^-$ . If this anodic dissolution process is stable and localized, some corrosion pits would be formed. The cathodic reduction outside the pits would take place as:  $\text{O}_2 + 2\text{H}_2\text{O} + 4\text{e}^- \rightarrow 4\text{OH}^-$  and  $2\text{H}^+ + 2\text{e}^- \rightarrow \text{H}_2$ . The hydrolysis of the aluminum chlorides induces local acidification of the solution in the pits as follows:



Thus, the solution on the bottom of the pits becomes more aggressive, and typical auto-propagation pitting corrosion is established on the substrate surface. The influence of the barrier effect of PEO coating on corrosion process mainly displays two aspects. On the one hand, the coating limits the transportation of the corrosive solution toward the substrate and restrains the electrochemical corrosion on the substrate surface, which is well known as the main anti-corrosion mechanism of the PEO coating. On the other hand, the coating will also establish a barrier to diffusion of  $\text{H}^+$  ions,  $\text{Al}^{3+}$  ions and other product ions and help pits to develop by maintaining a concentrated pit anolyte. With the propagation of pitting corrosion, the  $\text{Al}^{3+}$  ions will diffuse outward because of the existence of concentration gradient and will be hydrolyzed to  $\text{Al}(\text{OH})_3$  precipitate. In the case of pitting corrosion of bare aluminum specimen, the corrosion products usually precipitate along the rim of the pitting cavities (Ref 36), as shown in Fig. 7(a). For the PEO specimens, however, the corrosion products are accumulated gradually and block the mouth of the pits due to the barrier effect of PEO coatings, as shown in Fig. 7(b). This hinders the exchange of ions, especially the entrance of  $\text{Cl}^-$  ions into the pits. So the corrosion products can be regarded as a protective layer limiting the further corrosion of the substrate.

The EIS results also reveal the existence of corrosion products in the pits. After 720-h immersion, the EC turns into the circuit as shown in Fig. 5(c). The elements  $L$  and  $R_L$  in the circuit indicate the active corrosion product ions adsorbed in the pits. It should be noted that pitting corrosion begins far earlier than 720 h. The EC of 40 h and 150 h does not change into Fig. 5(c), probably because the density and size of the pits are not enough to cause the EC to change. From the EIS plots in

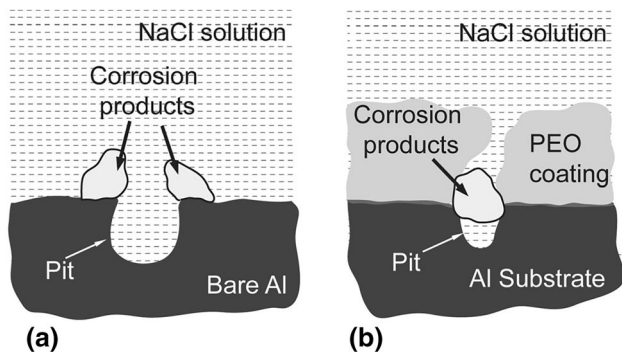


**Fig. 7** Schematic representation of the barrier effect of the PEO coating that accumulates corrosion products inside the pits and the pores next to the pits. (a) A pit and corrosion product on bare aluminum; (b) a pit and corrosion product on PEO-coated aluminum

Fig. 4(e) and (g), it can be seen that the corrosion resistance at low frequency decreases evidently after 720-h immersion, which indicates that the active surface in the pits contributes much less to the corrosion resistance compared to the compact interface. However, the value of  $R_1$  increased at 720 h compared to that at 150 h as shown in Fig. 6, which indicates that some corrosion products in the pits and pores increase the corrosion resistance of the outer porous layer.

**3.2.3 Repetitive Polarization Test.** Repetitive polarization test is employed to fabricate a kind of “artificial pit” for the migration of ions in the pits. The original “artificial-pit” technique fabricating a dissolving surface on the cross section of metal wires to simulate corrosion pits through repetition of cyclic potentiodynamic polarization or potentiostatic test was described previously (Ref 34, 35). Figure 8 shows the 1st, 5th, 8th, 10th and 12th cycles of the repetitive polarization measurements. It can be seen that the breakdown potential of the specimen is about  $-0.6$  V. The anodic polarization from  $-0.6$  to  $0.2$  V is to accelerate the generation of pitting corrosion. Although the pits develops slowly and could not form a dissolving surface through the test because of the protection of the PEO coating, these pits under the defects (pores and cracks) of the coating have similar geometrical configuration to wire “artificial pit” (Ref 35). Then, on the backward sweep of each cycle, the pits will be re-passivated at  $-0.85$  V. Moreover, a cathodic peak appears at about  $-1.1$  V during the cathodic polarization in each curve in the figure except the first cycle, and the amplitude of the peak becomes greater and its position shifts to more negative potentials as the number of the polarization cycle increases. In addition, compared to the first cycle, the  $E_{\text{corr}}$  of the other curves shifts negatively for  $0.28$ – $0.37$  V as shown in Fig. 8. This shift of the  $E_{\text{corr}}$  may be induced by the composition change in the solution near the specimen caused by the intensive corrosion reaction during the anodic polarization.

Figure 9 depicts the geometry of an “artificial pit” on a PEO-coated specimen with its qualitative concentration profiles of  $\text{H}^+$  ions during the repetitive polarization process. With the anodic polarization going on, more and more  $\text{Al}^{3+}$  ions are generated, and a large number of  $\text{H}^+$  ions are produced by the hydrolysis of  $\text{Al}^{3+}$  ions, as shown in Eq 1, 2, and 3. Because of the diffusion barrier effect of the PEO coating, the concentra-

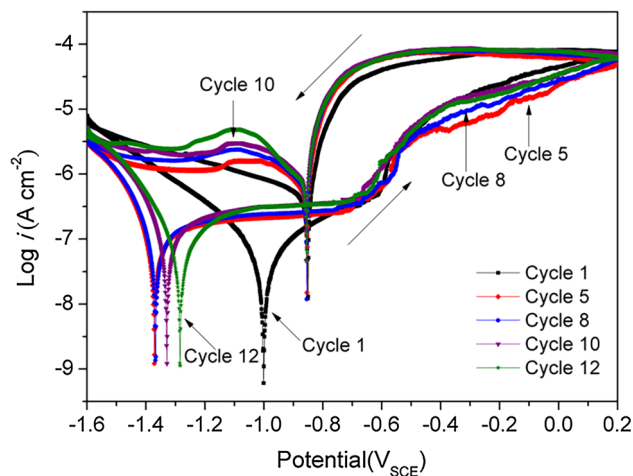


**Fig. 8** Repetitive polarization measurements of PEO-coated specimen in 3.5 wt.% NaCl solution

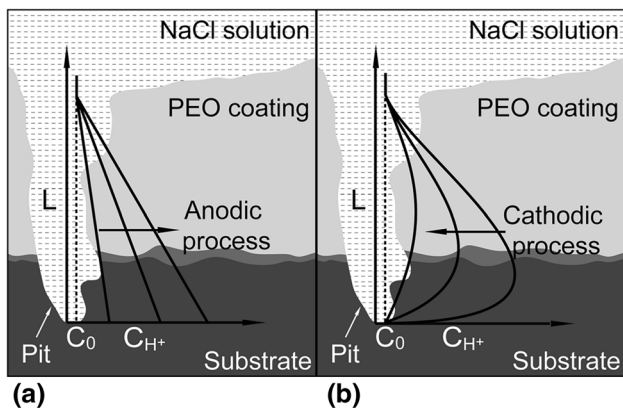


**Fig. 9** A schematic of the artificial-pit geometry together with qualitative concentration profiles of hydrogen ions along the coating depth during (a) anodic and (b) cathodic polarizations

tion of  $H^+$  ions is considered to be a gradient along the thickness of coatings and the depth of pits, and higher concentration of  $H^+$  ions should be detected near the bottom of the pits due to its close location to the Al substrate. And the concentration of  $H^+$  ions increases with anodic polarization time, so the slope of the pore depth–hydrogen concentration curve should decrease with the anodic polarization time (shown in Fig. 9a). When the cathodic polarization begins, these  $H^+$  ions become hydrogen gas; thus, the concentration of  $H^+$  ions has a tendency to decrease. As the potential scans into negative direction, the reduction rate of the  $H^+$  ions keeps increasing and reaches a cathodic peak at  $-1.1$  V. Besides the reduction reaction, their out diffusion also leads to the decrease in the concentration of  $H^+$  ions at the mouths of the pores. Thus, the concentration profile in Fig. 9(b) shows a maximum in the pits and its height decreases with cathodic polarization time. The concentration of the  $H^+$  ions increases with cycles of anodic polarization due to the development of the pits and the limitation effect of the PEO coating. Consequently, a cathodic current peak is generated by the reaction of hydrogen evolution inside the pits with the cathodic polarization, and the amplitude of the peak becomes greater as the number of cycle increases.

## 4. Conclusions

The effect of the PEO coating on the corrosion process of aluminum in 3.5 wt.% NaCl solution is investigated in the present work. Some conclusions can be obtained as follows:

1. In the initial period of the immersion treatment, the aggressive solution penetrates through the coating as a diffusion process and the main effect of the PEO coating is a physical shield.
2. After sufficient immersion time, pitting corrosion takes place at some vulnerable regions. PEO coatings have two roles, i.e., a physical shield and a porous surface layer. The former prevents the exposed area of the substrate to corrode, while the latter helps pitting corrosion take place and develop by maintaining a concentrated pit anolyte.
3. With the pits growing, corrosion products accumulate inside the pits and the pores next to the pits, which act as a protective layer.

## Acknowledgments

This work was supported by National Natural Science Foundation of China (Nos. 51671167 and 51171167) and Hebei Province Natural Science Foundation of China (Nos. 2015203348 and B2015203406).

## Reference

1. A.L. Yerokhin, X. Nie, A. Leyland, A. Matthews, and S.J. Dowey, Plasma Electrolysis for Surface Engineering, *Surf. Coat. Technol.*, 1999, **122**(2-3), p 73–93
2. J. Liang, P.B. Srinivasan, C. Blawert, M. Störmer, and W. Dietzel, Electrochemical Corrosion Behaviour of Plasma Electrolytic Oxidation Coatings on AM50 Magnesium Alloy Formed in Silicate and Phosphate Based Electrolytes, *Electrochim. Acta*, 2009, **54**(14), p 3842–3850
3. M. Vakili-Azghandi, A. Fattah-alhosseini, and M.K. Keshavarz, Effects of  $Al_2O_3$  Nano-Particles on Corrosion Performance of Plasma Electrolytic Oxidation Coatings Formed on 6061 Aluminum Alloy, *J. Mater. Eng. Perform.*, 2016, **25**(12), p 5302–5313
4. A. Khakzad, S.M. Mousavi Khoi, S.A. Tayebifard, E. Aghaie, Y. Behnamian, M. Mozammel, and H. Maleki-Ghaleh, Alumina-Silica Composite Coatings on Aluminum by Plasma Electrolytic Oxidation: The Effect of Coating Time on Microstructure, Phase, and Corrosion Behavior, *J. Mater. Eng. Perform.*, 2017, **26**(6), p 2663–2670
5. J. Liang, P.B. Srinivasan, C. Blawert, and W. Dietzel, Influence of Chloride Ion Concentration on the Electrochemical Corrosion Behaviour of Plasma Electrolytic Oxidation Coated AM50 Magnesium Alloy, *Electrochim. Acta*, 2010, **55**(22), p 6802–6811
6. R. Arrabal, E. Matykina, P. Skeldon, and G.E. Thompson, Incorporation of Zirconia Particles Into Coatings Formed on Magnesium by Plasma Electrolytic Oxidation, *J. Mater. Sci.*, 2008, **43**(5), p 1532–1538
7. A. Fattah-alhosseini, S.O. Gashti, and M. Molaie, Effects of Disodium Phosphate Concentration ( $Na_2HPO_4 \cdot 2H_2O$ ) on Microstructure and Corrosion Resistance of Plasma Electrolytic Oxidation (PEO) Coatings on 2024 Al Alloy, *J. Mater. Eng. Perform.*, 2018, **27**(2), p 825–834
8. A. Sharma, Y.-J. Jang, and J.P. Jung, Effect of KOH to  $Na_2SiO_3$  Ratio on Microstructure and Hardness of Plasma Electrolytic Oxidation Coatings on AA 6061 Alloy, *J. Mater. Eng. Perform.*, 2017, **26**(10), p 5032–5042
9. R.C. Barik, J.A. Wharton, R.J.K. Wood, K.R. Stokes, and R.L. Jones, Corrosion, Erosion and Erosion–Corrosion Performance of Plasma Electrolytic Oxidation (PEO) Deposited  $Al_2O_3$  Coatings, *Surf. Coat. Technol.*, 2005, **199**(2-3), p 158–167
10. K. Du, X. Guo, Q. Guo, Y. Wang, F. Wang, and Y. Tian, Effect of PEO Coating Microstructure on Corrosion of Al 2024, *J. Mater. Eng. Perform.*, 2012, **159**(12), p C597–C606
11. D.Y. Hwang, M.K. Yong, D.Y. Park, B. Yoo, and H.S. Dong, Corrosion Resistance of Oxide Layers Formed on AZ91 Mg Alloy in  $KMnO_4$  Electrolyte by Plasma Electrolytic Oxidation, *Electrochim. Acta*, 2009, **54**(23), p 5479–5485
12. G.H. Lv, H. Chen, X.Q. Wang, and H. Pang, Effect of Additives on Structure and Corrosion Resistance of Plasma Electrolytic Oxidation Coatings on AZ91D Magnesium Alloy in Phosphate Based Electrolyte, *Surf. Coat. Technol.*, 2010, **205**(7), p S36–S40
13. H. Duan, C. Yan, and F. Wang, Effect of Electrolyte Additives on Performance of Plasma Electrolytic Oxidation Films Formed on Magnesium Alloy AZ91D, *Electrochim. Acta*, 2007, **52**(11), p 3785–3793
14. J. Liang, P.B. Srinivasan, C. Blawert, and W. Dietzel, Influence of pH on the Deterioration of Plasma Electrolytic Oxidation Coated AM50 Magnesium Alloy in NaCl Solutions, *Corros. Sci.*, 2010, **52**(2), p 540–547
15. H. Khanmohammadi, S.R. Allahkaram, A. Igual Munoz, and N. Towhidi, The Influence of Current Density and Frequency on the Microstructure and Corrosion Behavior of Plasma Electrolytic Oxidation Coatings on Ti6Al4V, *J. Mater. Eng. Perform.*, 2017, **26**(2), p 931–944
16. D. Sreekanth, N. Rameshbabu, K. Venkateswarlu, C. Subrahmanyam, L.R. Krishna, and K.P. Rao, Effect of  $K_2TiF_6$  and  $Na_2B_4O_7$  as



- Electrolyte Additives on Pore Morphology and Corrosion Properties of Plasma Electrolytic Oxidation Coatings on ZM21 Magnesium Alloy, *Surf. Coat. Technol.*, 2013, **222**(6), p 31–37
17. D.A. Becerik, A. Ayday, L.C. Kumruoğlu, S.C. Kurnaz, and A. Özel, The Effects of Na<sub>2</sub>SiO<sub>3</sub> Concentration on the Properties of Plasma Electrolytic Oxidation Coatings on 6060 Aluminum Alloy, *J. Mater. Eng. Perform.*, 2011, **21**(7), p 1426–1430
  18. M. Roknian, A. Fattah-alhosseini, and S.O. Gashti, Plasma Electrolytic Oxidation Coatings on Pure Ti Substrate: Effects of Na<sub>3</sub>PO<sub>4</sub> Concentration on Morphology and Corrosion Behavior of Coatings in Ringer's Physiological Solution, *J. Mater. Eng. Perform.*, 2018, **27**(3), p 1343–1351
  19. L. Wen, Y. Wang, Y. Zhou, L. Guo, and J.H. Ouyang, Microstructure and Corrosion Resistance of Modified 2024 Al Alloy Using Surface Mechanical Attrition Treatment Combined with Microarc Oxidation Process, *Corros. Sci.*, 2011, **53**(1), p 473–480
  20. L. Pezzato, K. Brunelli, R. Babolin, P. Dolcet, and M. Dabalà, Sealing of PEO Coated AZ91 Magnesium Alloy Using La-Based Solutions, *Int. J. of Corros.*, 2017, **2017**(3), p 1–13
  21. M. Mohedano, C. Blawert, and M.L. Zheludkevich, Cerium-Based Sealing of PEO Coated AM50 Magnesium Alloy, *Surf. Coat. Technol.*, 2015, **269**(1), p 145–154
  22. L.Y. Cui, S.D. Gao, P.P. Li, R.C. Zeng, F. Zhang, S.Q. Li, and E.H. Han, Corrosion Resistance of a Self-Healing Micro-Arc Oxidation/Polymethyltrimethoxysilane Composite Coating on Magnesium Alloy AZ31, *Corros. Sci.*, 2017, **118**, p 84–95
  23. C. Wang, J. Shen, F. Xie, B. Duan, and X. Xie, A Versatile Dopamine-Induced Intermediate Layer for Polyether Imides (PEI) Deposition on Magnesium to Render Robust and High Inhibition Performance, *Corros. Sci.*, 2017, **122**, p 32–40
  24. C.N. Cao and J.Q. Zhang, *An Introduction of Electrochemical Impedance Spectroscopy Science*, 2002, p 86–106
  25. Y. Zhang, C. Yan, F. Wang, and W. Li, Electrochemical Behavior of Anodized Mg Alloy AZ91D in Chloride Containing Aqueous Solution, *Corros. Sci.*, 2005, **47**(11), p 2816–2831
  26. Y. Zhang, Y. Wu, D. Chen, R. Wang, D. Li, C. Guo, G. Jiang, D. Shen, S. Yu, and P. Nash, Micro-Structures and Growth Mechanisms of Plasma Electrolytic Oxidation Coatings on Aluminium at Different Current Densities, *Surf. Coat. Technol.*, 2017, **321**, p 236–246
  27. D. Chen, R. Wang, Z. Huang, Y. Wu, Y. Zhang, G. Wu, D. Li, C. Guo, G. Jiang, S. Yu, D. Shen, and P. Nash, Evolution Processes of the Corrosion Behavior and Structural Characteristics of Plasma Electrolytic Oxidation Coatings on AZ31 Magnesium Alloy, *Appl. Surf. Sci.*, 2018, **434**, p 326–335
  28. V. Dehnavi, B.L. Luan, D.W. Shoesmith, X.Y. Liu, and S. Rohani, Effect of Duty Cycle and Applied Current Frequency on Plasma Electrolytic Oxidation (PEO) Coating Growth Behavior, *Surf. Coat. Technol.*, 2013, **226**(8), p 100–107
  29. R.O. Hussein, X. Nie, D.O. Northwood, A. Yerokhin, and A. Matthews, Spectroscopic Study of Electrolytic Plasma and Discharging Behaviour During the Plasma Electrolytic Oxidation (PEO) Process, *J. Phys. D Appl. Phys.*, 2010, **43**(10), p 105203–105215
  30. X. Nie, E.I. Meletis, J.C. Jiang, A. Leyland, A.L. Yerokhin, and A. Matthews, Abrasive Wear/Corrosion Properties and TEM Analysis of Al<sub>2</sub>O<sub>3</sub> Coatings Fabricated Using Plasma Electrolysis, *Surf. Coat. Technol.*, 2002, **149**(2–3), p 245–251
  31. F. Monfort, A. Berkani, E. Matykina, P. Skeldon, G.E. Thompson, H. Habazaki, and K. Shimizu, Development of Anodic Coatings on Aluminium Under Sparking Conditions in Silicate Electrolyte, *Corros. Sci.*, 2007, **49**(2), p 672–693
  32. C. Liu, D. He, Q. Yan, Z. Huang, P. Liu, D. Li, G. Jiang, H. Ma, P. Nash, and D. Shen, An Investigation of the Coating/Substrate Interface of Plasma Electrolytic Oxidation Coated Aluminum, *Surf. Coat. Technol.*, 2015, **280**, p 86–91
  33. Y. Wang, Z. Huang, Q. Yan, C. Liu, P. Liu, Y. Zhang, C. Guo, G. Jiang, and D. Shen, Corrosion Behaviors and Effects of Corrosion Products of Plasma Electrolytic Oxidation Coated AZ31 Magnesium Alloy Under the Salt Spray Corrosion Test, *Appl. Surf. Sci.*, 2016, **378**, p 435–442
  34. J.W. Tester and H.S. Isaacs, Diffusional Effects in Simulated Localized Corrosion, *J. Electrochem. Soc.*, 1975, **122**(11), p 1438–1445
  35. C. Vargel, M. Jacques, and M.P. Schmidt, *Corrosion of Aluminium*, 2004, p 81–109
  36. K. Sasaki and H.S. Isaacs, Origins of Electrochemical Noise during Pitting Corrosion of Aluminum, *J. Electrochem. Soc.*, 2004, **151**(3), p B124–B133

**Publisher's Note** Springer Nature remains neutral with regard to jurisdictional claims in published maps and institutional affiliations.